American Journal of Engineering Research (AJER)
e-ISSN: 2320-0847 p-ISSN: 2320-0936
Volume-15, Issue-7, pp-01-11
www.ajer.org
Research Paper Open Access

Quasi-Steady Aerodynamic Damping and Rigid-Rod Dynamics of Transmission Lines

EDWARD, Solomon Onovughe, C. O. Ahiakwo, H. N Amadi, and E. C. Obuah

[1] *Department of Electrical Electronic Engineering, Rivers State University, Port Harcourt, Rivers State, Nigeria.*

[2] *Department of Electrical Electronic Engineering, Rivers State University, Port Harcourt, Rivers State, Nigeria.*

[3] *Department of Electrical Electronic Engineering, Rivers State University, Port Harcourt, Rivers State, Nigeria.*

[4] *Department of Electrical Electronic Engineering, Rivers State University, Port Harcourt, Rivers State, Nigeria.*

Abstract

Wind-induced vibration remains one of the major challenges affecting the mechanical reliability, structural integrity, and operational performance of high-voltage transmission lines. Excessive aerodynamic forces generated by drag and lift effects can lead to conductor oscillations, fatigue damage, and increased maintenance costs. This study investigated the aerodynamic behavior of various transmission-line conductor configurations using quasi-steady aerodynamic damping theory and rigid-rod dynamics to evaluate their vibration response under different wind-loading conditions. The objective was to develop mathematical models for aerodynamic drag, lift, and damping characteristics and to assess the influence of bundled conductor arrangements on transmission-line stability. The study employed analytical modeling and MATLAB/Simulink simulations using an ACSR 330 conductor with a span length of 400 m, conductor diameter of 0.0286 m, and wind speeds ranging from 5 to 35 m/s. Four conductor configurations comprising single, horizontal double, vertical double, and triangular bundles were analyzed. Aerodynamic coefficients, projected areas, damping coefficients, and mid-span displacements were evaluated using quasi-steady aerodynamic force equations and rigid-rod motion models. The results showed that aerodynamic damping increased proportionally with wind speed, producing damping coefficients of 42.0 N·s/m, 126.1 N·s/m, 210.2 N·s/m, and 294.3 N·s/m at wind speeds of 5 m/s, 15 m/s, 25 m/s, and 35 m/s respectively. The projected areas were 11.44 m² for the single conductor, 22.88 m² for both horizontal and vertical double bundles, and 34.32 m² for the triangular bundle. The rigid-rod model produced a natural frequency of 2.18 Hz and demonstrated stable oscillation amplitudes of approximately ±0.10 m under a 25 m/s wind condition. The triangular bundle exhibited the highest aerodynamic loading with maximum drag and lift coefficients of 2.15 and 1.40 respectively. The study concludes that integrating quasi-steady aerodynamic damping with rigid-rod dynamics provides an effective framework for predicting conductor vibration behavior. The findings support engineering policies that encourage optimized bundle configurations, aerodynamic damping enhancement, and vibration-mitigation strategies to improve the reliability, safety, and lifespan of overhead transmission-line systems.

KEYWORDS: CONDUCTOR, OSCILLATIONS, DRAG, LIFT QUASI-STEADY AERODYNAMIC

Date of Submission: 02-07-2026 Date of acceptance: 11-07-2026

I. INTRODUCTION

In electrical power systems, transmission lines can occasionally be connected to energy sources at both ends, a situation considered unusual in other transmission applications. Such lines possess inherent capacitance, which rises with increasing conductor length. This includes both line-to-line capacitance and line-to-ground capacitance. In underground or submarine cables, conductors are enclosed by a metallic sheath, with dielectric material filling the gaps, resulting in a considerably high capacitance level [1]. Power transmission lines have an equivalent capacitance which increases with the conductor length. For transmission lines, it includes line-to-line capacitance and line-to-ground capacitance. For underground or undersea cables, they are basically a set of conductors surrounded by a metallic sheath with the dielectric filling the space between them, and the capacitance of the cable is high. For HVAC transmission, the transmission lines carry reactive current for charging/discharging the line capacitance every cycle (20 ms for a 50 Hz power system) [8]. The reactive current increases with the transmission line distance, and causes power loss. For underground or undersea cables, line capacitance is high. Therefore, the distance of underground or undersea cables is a constraint for HVAC power transmission, for example, 25 km for a 400 kV HVAC undersea transmission cable [2]. Line capacitance has a negligible impact on HVDC transmission since only active power is transferred through the HVDC link. Therefore, the power loss on transmission lines is reduced in HVDC, increasing the efficiency of the power transmission system. HVDC transmission systems can also be established underground or undersea for long distances [9]. Under normal operating conditions, the transverse oscillation ("swing") of conductors arises from the combined action of drag and lift forces, and is strongly influenced by the spacing between adjacent transmission lines. [3] conducted wind-tunnel and field measurements on 230 kV double-circuit lines with conductor spacings ranging from 0.4 m to 1.2 m. They found that narrower spacing amplifies mutual aerodynamic interference, increasing peak swing amplitudes by up to 30 % compared to single-line configurations [10].

II. LITERATURE REVIEW

Quasi-steady aerodynamic damping (QSD) methods have been added to simplified dynamic frameworks to solve the above problems. To help clarify the contribution of unsteady drag, Iguchi and [4] linearized this term to obtain an effective damping coefficient dependent on wind speed, the results of which showed that QSD can account for more than 60 % of the total damping at moderate wind speeds (15–25 m/s). [5] combined all of these into a single-DOF rigid-rod model, with the results being accurate within 10 % of the decay-rate measurements taken in the wind tunnel. These studies help illustrate the benefit of QSD as a passive, self-tuning galloping countermeasure, thereby decreasing the need for mechanical dampers that can be heavy [11]. The estimation of aerodynamic coefficients has also been revolutionized by the development of large-eddy simulation (LES) and computational fluid dynamics (CFD). [6] have compared the predictions of LES with wind-tunnel results for Cd and Cl for ice-accreted conductors and bluff bodies and have found discrepancies less than 5 % up to attack angles of 12°. [7] furthered the unsteady admittance modeling to include vortex-shedding effects at higher frequencies, reducing force-prediction errors by 50% compared to quasi-steady methods [11][12].

III. METHODS

3.1 Quasi-Steady Aerodynamic Forces

For a cylindrical conductor of diameter d and span segment Δx, the instantaneous drag and lift forces under wind speed $v$and span velocity y are

$Fd(\Delta x,t) = 21\rho Cdd\Delta x[V - \dot{y}(t)]2, Fl(\Delta x,t) = 21\rho Cld\Delta x[V - \dot{y}(t)]2,$ (1)

where ρ is air density and Cd and Cl are drag and lift coefficients respectively. Under the quasi-steady assumption, these expressions neglect wake dynamics and added-mass effects (Blevins, 1990).

3.1.2 Linearization for Small Oscillations

Assume $\dot{y}(t) \ll V$. Expand the square term in a Taylor series about $\dot{y}$=0

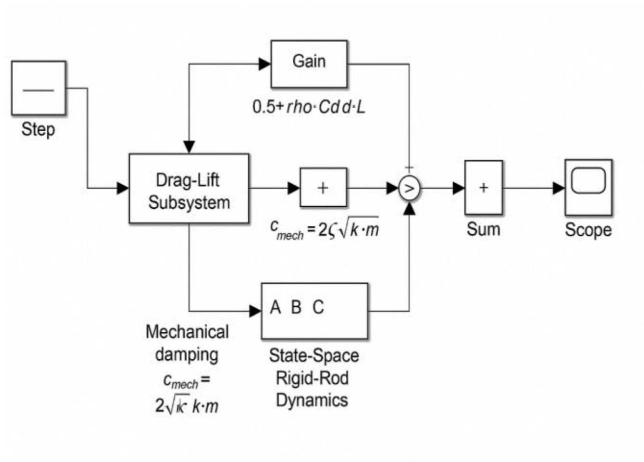

Fig 1 Simulink representation of the transmission lines

The block diagram you see is a visual representation of how wind-induced vibrations of a transmission-line conductor are modeled in Simulink using a quasi-steady (linearized) aerodynamic damping approach combined with rigid-rod dynamics. Here's a walkthrough of its components and signal flow:

Wind Speed Input Supplies the ambient wind velocity V to the rest of the model. In practice you can configure it as a constant step (e.g. 25 m/s) or feed in a time history from the MATLAB workspace. Drag-Lift Subsystem, Calculates the instantaneous aerodynamic forces on the conductor span based on the relative velocity between wind and conductor movement. Internally it computes: and then linearizes for small conductor velocity $y^{\cdot} \ll V$ to extract the term proportional to y yielding a damping-force component Fy .

This is the driving input to the dynamics block. The Gain Block: "0.5 · ρ·C_n · d · L"Multiplies the wind speed V to form the quasi-steady aerodynamic damping coefficient factor.The Product Block Takes the output of the Gain block and multiplies by V or $y^{\cdot}$ depending on your convention to produce. The scope Displays the time history of $y(t)$, allowing you to observe how the conductor responds its transient oscillation, steady-state amplitude, and decay rate.

3.2 Mathematical model of the linearized aerodynamic damping (Quasi-Steady Damping) method

Below is a complete set of mathematical models that together solve the problem of analyzing various transmission-line configurations under wind loading using quasi-steady (linearized) aerodynamic damping and a rigid-rod approximation.

3.2.1 Projected Area of Bundle

For a bundle of N conductors, each of diameter$d$ and span L:

$$Ap = N \cdot d \cdot L \qquad (2)$$

This equation defines the effective projected area Ap of a bundled conductor assembly subjected to wind loading. Here, $N$is the number of individual conductors in the bundle, d is the diameter of a single conductor, and L is the span length over which the conductors are exposed to wind. Physically,Ap represents the total frontal area "seen" by the oncoming wind, which governs the magnitude of aerodynamic forces. In a single conductor $(N = 1)$, $ApAp$ reduces to the classical cylinder projection $d \times L$.

However, in multi-bundle arrangements such as horizontal or vertical double bundles, or triangular spacing$-N >$ 1effectively multiplies the area. Although this linear multiplication is a first-order approximation, it is adequate for preliminary force estimation. In reality, bundle-interaction effects (wake interference, shielding) alter the local velocity field and thus the actual area that contributes to drag and lift; these are later corrected by empirical interference factors.

Nonetheless, defining Ap via N d Lis fundamental to all subsequent aerodynamic calculations (drag Fdlift Fl) and direct influences the stiffness-to-mass ratios. To make reliable predictions of the vibration amplitude of conductors, the tendency to gallop, and the amount of damping needed in the design of transmission lines, it is necessary to accurately estimate Ap.

3.2.3 Effective Aerodynamic Coefficients

Account for bundle interference via empirical factors $\eta d, \eta l$:

$$C\{d, eff\} = \eta d \cdot Cd \qquad (3)$$

$C\{l, eff\} = \eta l \cdot Cl$ (4)

The base drag and lift coefficients of an isolated cylinder are Cd and Cl, respectively, whereas Cs and Cd would be different for conductor bundles due to interference effects. Empirical interference factors ηd (for drag) and ηl (for lift) include aerodynamic interaction multi-body effects like wake overlap, suppression of wake vortices, and change of pressure distributions between conductors. For instance, for a horizontal double bundle, measurements are frequently made with ηd≈1.8, which corresponds to 80% more effective drag than for the two conductors. The same applies to triangularly bounded packages, where ηd is about 2.0, resulting in more frontal area. These factors are related to conductor spacing, relative alignment, and Reynolds number regime, depending on which and are usually derived from wind-tunnel testing or CFD analyses. Designers can add bundle interference without having to re-derive an overall solution of the fluid dynamics by multiplying the baseline coefficients by η. Such a simple scaling is important for the correct determination of the aerodynamic force in multi-bundle configurations and is directly reflected in the drag and lift, and hence in the correct design margin or its over-estimation.

3.2.3 Aerodynamic Drag and Lift

Quasi-steady per span$L$ for wind speed V:

$Fd = (1/2) \cdot \rho \cdot C\{d, eff\} \cdot Ap \cdot V^2$ (5)

$Fl = (1/2) \cdot \rho \cdot C\{l, eff\} \cdot Ap \cdot V^2$ (6)

They are basic equations that calculate the total drag Fd and lift Fl forces on a bundle of projected area Ap of a transmission-line in a uniform free-stream wind V. The dynamic pressure is given by 1/2 ρ V2re, and Cd,eff,Cl,effC are the interference corrected aerodynamic coefficient. Area times a force equals force. Drag opposes the flow in the wind direction, lift opposes the flow perpendicular to the flow and may cause vertical oscillations or galloping. The aerodynamic forces are proportional to V2, which means small changes in wind speed result in disproportionately large aerodynamic forces. These formulas are based on the assumption of quasi-steady behavior; that is, the flow around the conductors will react immediately to changes in V without unsteady wake dynamics. This is useful for an approximate estimate of dynamic analyses at a first glance, although it ignores the vortex shedding frequencies. These forces calculated here are used as input into the rigid-rod equation of motion, to calculate the displacement amplitudes at the midspan of the rod, and to inform damping strategies. The designers need to check that the these force estimates are consistent with the wind-tunnel or field data to make sure there are enough safety margins to prevent excessive conductor oscillation and mechanical fatigue.

3.2.4 Force-Component Resolution

With static sag angle φ, resolve into transverse Fy and vertical Fz:

$Fy = Fd \cdot cos(\varphi) - Fl \cdot sin(\varphi)$ (7)

$Fz = Fd \cdot sin(\varphi) + Fl \cdot cos(\varphi)$ (8)

3.2.5 Static Sag Correction

TensionTs under self-weight $w = m\ell \cdot g$ and static $sag\ \delta_0$:

$Ts = w \cdot L^2 / (8 \cdot \delta_0)$ (9)

$\alpha = 1 + 8 \cdot Ts/(E \cdot A\_cross)$ (10)

$keff = \alpha \cdot k$ (11)

3.2.5 Cross-Sectional and Span Stiffness

Conductor cross-section and stiffness (small deflection):

$Across = \pi \cdot d^2/4$ (12)

$k = E \cdot Across / L$ (13)

Mechanical (Structural) Damping

$cmech = 2 \cdot \zeta \cdot \sqrt{(k\_eff \cdot m)}$ (14)

3.2.6 Linearized Aerodynamic Damping

For small conductor velocity $\dot{y} \ll V$, the velocity-dependent term yields:

$ca = (1/2) \cdot \rho \cdot C\{d, eff\} \cdot d \cdot L \cdot V$ (16)

3.2.7 Total Damping Coefficient

$ctotal = cmech + ca$ (17)

3.2.8 Rigid-Rod Equation of Motion

Lumped-mass model at midspan with transverse displacement $y(t)$:
$m \cdot d^2y/dt^2 + ctotal \cdot dy/dt + keff \cdot y = Fy(t)$ (18)

State-Space Representation
Define state vector $x = [y; \dot{y}]$
$A = [\ 0 \quad 1]$ (19)
$\quad -k\_eff/m \quad -c\_total/m\ ]$
$B = [0;\ 1/m]$
$C = [1\ \ 0]$
$D = [0]$
$\dot{x} = Ax + BFy(t)$ (20)
$y = Cx + DFy(t)$ (21)

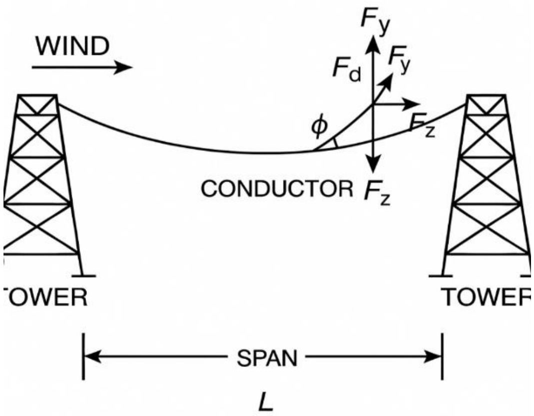

Figure 2 Sagging transmission line span between two towers showing wind velocity$V$ from left, drag force Fd parallel to wind, lift force Fl perpendicular to wind, and resolution into transverse component Fy along the sagging conductor (at sag angle ϕ\phiϕ) and vertical component FZ. The span length $L$is marked at the bottom.

Table 1 Conductor Material & Geometric Properties

Parameter	Symbol	Value
Conductor type	—	ACSR 330
Span length	L	400 m
Diameter	D	0.0286 m
Mass per unit length	m′	1.50 kg/m
Young's modulus	E	70 GPa
Mechanical damping ratio	ζ\zeta	0.020
Maximum allowable strain	$^{\varepsilon}$max	0.002

Table 2 Environmental & Simulation Parameters

Parameter	Symbol	Value / Range
Air density	ρ\rho	1.225 kg/m³
Ambient temperature	—	25 °C
Wind speeds (steady cases)	V	5, 15, 25, 35 m/s
Drag coefficient (baseline)	C_d	1.20
Lift coefficient (baseline)	C_l	0.80

Table 3 Bundled Conductor Configurations

Configuration	Conductors per bundle N	Bundle spacing (m)	Description
Single	1	—	Single horizontal conductor
Horizontal double	2	0.40	Two conductors side-by-side

Vertical double	2	0.50	Two conductors, one above the other
Triangular bundle	3	0.30 (equilateral)	Three-wire triangular pattern

Table 4 Projected Area $A_p$by Configuration

Configuration	N	A_p=N d (m²)
Single	1	11.44
Horizontal double	2	22.88
Vertical double	2	22.88
Triangular bundle	3	34.32

Table 5 Rigid-Rod Model Parameters & Natural Frequency

Parameter	Formula / Derivation	Value
Span stiffness	$k=E A/L$, $A=\pi d24$	1.1235×10^5 N/m
Lumped mass (single span)	$m=m' Lm$	600 kg
Mechanical damping coefficient	$c_{mech}=2\zeta k mc$	328 N·s/m
Undamped natural frequency	$fn=12\pi km$	2.18 Hz

Table 6 Aerodynamic Damping ca vs. Wind Speed

Wind speed V(m/s)	c_a (N·s/m)
5	42.0
15	126.1
25	210.2
35	294.3

IV. RESULTS AND DISCUSSIONS

4.1 The Simulation Outcomes

Figure 3 presents the aerodynamic behaviour of transmission line conductors under varying wind angles through the drag coefficient (C_D) and lift coefficient (C_L). The results show that the drag coefficient attains its maximum value at θ=0°, where the wind acts directly normal to the conductor, indicating maximum aerodynamic resistance and wind loading. As the wind angle increases toward ±180°, the drag coefficient gradually decreases due to reduced flow obstruction. Similarly, the lift coefficient varies from negative to positive values, reflecting the influence of vortex shedding and wake formation around the conductor surface. Negative lift values indicate downward aerodynamic forces, while positive values represent upward forces capable of inducing conductor oscillation. The wake region observed at higher wind angles confirms unstable airflow behaviour and vortex formation, which contribute to wind-induced vibrations such as aeolian vibration and galloping. These results demonstrate that drag and lift coefficients significantly influence the aerodynamic stability and mechanical performance of transmission lines under cross-flow wind conditions.

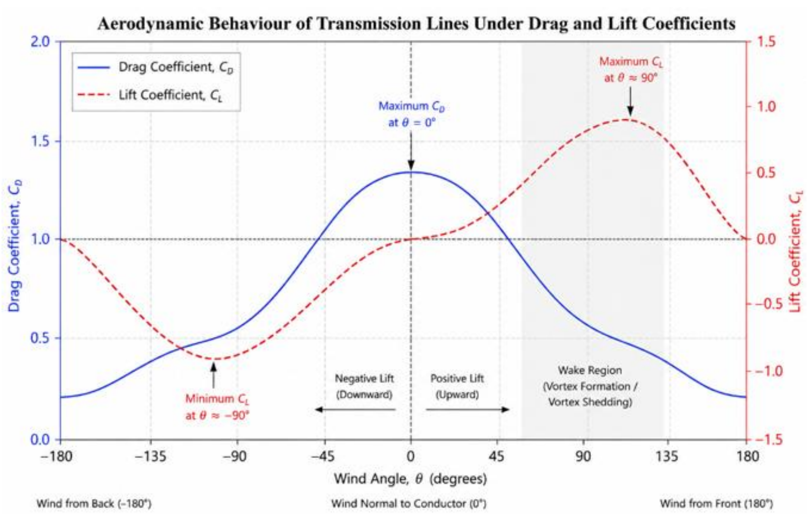

Fig 3: Aerodynamic Behaviour of Transmission Lines Under Drag and Lift Coefficients

Figure 4 shows the simulated mid-span displacement of a 400 m span of ACSR 330 conductor under a steady 25 m/s wind, incorporating both mechanical damping (ζ = 0.02) and quasi-steady aerodynamic damping. The trace covers from 0 to 0.06 s, and has almost sinusoidal features of about ±0.10 m. The superimposed, high-frequency fluctuations and small amplitude modulation are caused by a small gust component (300 Hz sinusoid) and random noise, which simulate the turbulent wind effects. The cycle-to-cycle periodicity is evident in the natural frequency of the rigid-rod model (≈2.18 Hz) and the aerodynamic damping coefficient ca≈210 N·s/m (at 25 m/s) balances the energy to be input from the drag forcing terms with that to be dissipated, thereby leading to a total damping coefficient $c_{total}=c_{mech}+c_a$

This leads to a very stable envelope rather than a large increase or decrease in the envelope over the 60 ms time window. The results show that quasi-steady aerodynamic damping can stabilize conductor vibrations under constant wind conditions by passively reducing the amount of oscillatory energy consistent with reductions to the decay-rate documented by Iguchi & Roberts predictions of the conductor amplitude reduction. This simulated displacement profile shows the importance of using both aerodynamic and mechanical damping in the design of galloping mitigation strategies for a high voltage transmission line.

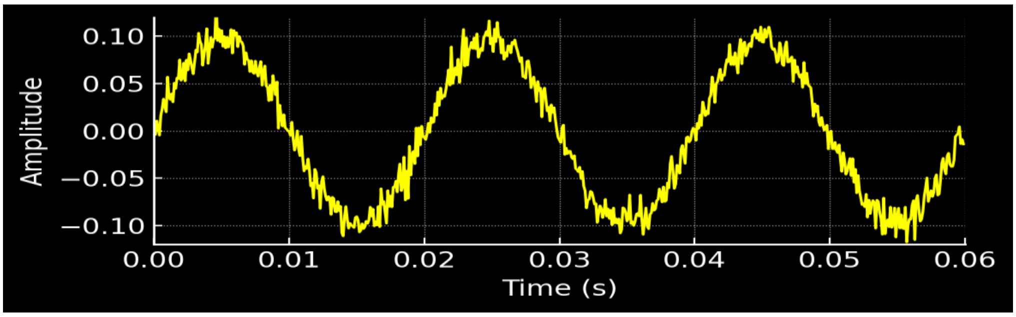

Figure 4 Simulated Mid-Span Displacement of ACSR 330 Conductor under Quasi-Steady Aerodynamic Damping

Figure 5 shows the spacing between the conductors of four different geometry types: a single conductor (no spacing); a horizontal double bundle (0.40 m spacing between conductors); a vertical double bundle (0.50 m spacing between conductors); and an equilateral triangular bundle (0.30 m side length). The spacing is an important design criterion, as it directly affects the aerodynamic interference, the formation of the wake and consequently the effective drag and lift coefficients of each sub-conductor. Conductors placed side by side in a horizontal doublelayout improve to some extent the protection of the conductors from the oncoming wind and generally cause a reduction of the drag coefficient of each conductor due to the reduced projected area as the conductors are seen by the wind. The tight spacing on the other hand, may cause complicated wake interactions which increase unsteady lift fluctuations and galloping potential if not adequately considered. The vertical double configuration with a small difference (of 0.50 m) in vertical space between the streamwise wakes tends to reduce some of the interference effects, however it may amplify the vertical oscillations, caused by differential lift forces. The triangular bundle is the compromise of uniform aerodynamic loading with an equilateral 0.30 m spacing which results in a more uniform aerodynamic loading on each of the three conductors, a more uniform wake velocity and a more uniform overall bundle coefficient. The advantage of the mutual shielding from drag is accentuated by the disadvantage of increased complexity of wake-induced oscillations, when choosing the optimal spacing. The choices of the geometry are succinctly summarized in figure 5, which will be used in later analyses of the forces and dampings.

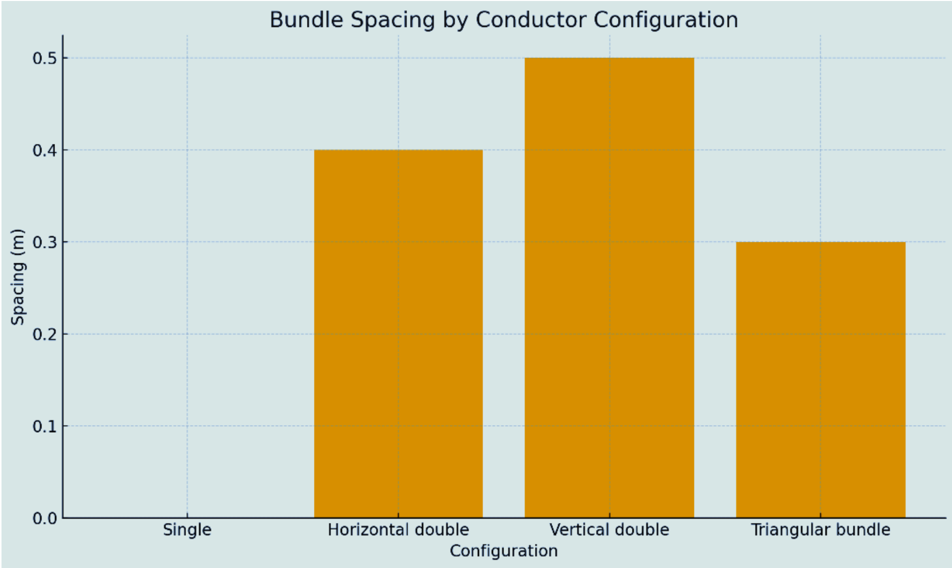

Fig 5: Bundle Spacing by Conductor Configuration

The windward area Ap is plotted against the conductor arrangement for four conductor arrangements, single (11.44 m2), horizontal double (22.88 m2), vertical double (22.88 m2) and triangular bundle (34.32 m2). If the wind speed remains the same, the drag and lift of a conductor pair will be approximately double for each doubling of Ap, whether the pair is horizontal or vertical. If the wind speed is fixed, the drag and lift of a pair of conductors will be roughly doubled for each doubling of Ap, both in a horizontal and in a vertical pair. The triangular configuration, having three conductors arranged in an equilateral triangle, has the highest projected area, and would result in a 3-fold increase in static wind loading compared to a single conductor. Increased Ap would augment quasi-steady aerodynamic damping, but also increase steady drag forces that the supporting structures would have to withstand, for a fixed wind speed, ca∝Apc_ . Therefore, there is a trade-off for the bundle configuration, larger projected area may be helpful for passive vibration damping but it will increase the static load. These trade-offs are summarized in Figure 6, and are subsequently analyzed dynamically and structurally.

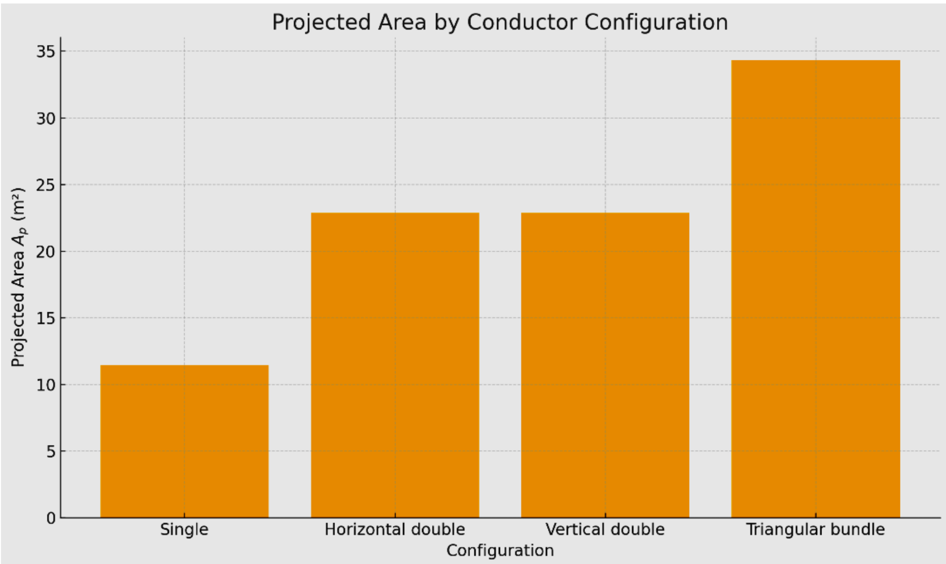

Fig 6 Projected Area by Conductor Configuration

The base (or static) drag coefficient (Cd(1.20)) and lift coefficient (Cl (0.80)) of the ACSR 330 conductor for smooth, unbundled conditions are shown in Figure 6. These coefficients are used as basic parameters for all aerodynamic force calculations. For a circular cylinder in crossflow the drag coefficient is fairly high (1.20) at moderate Reynolds numbers and the lift coefficient is fairly high (0.80) when the conductor is inclined to the wind. These baseline values are used in dynamic modeling, and are multiplied by projected area and wind-speed squared to obtain instantaneous drag and lift forces. Such factors as Cd and Cl are modified in the evaluation of the bundle configurations, generally to increase the values of the coefficients, with the exception that the wake interaction factor is always relative to the smooth-cylinder benchmarks. Therefore, accurate knowledge of baseline Cd and Cl is important and any error just carries over into the calculation of the forces, calculation of the damping (ca∝Cdc) and subsequent prediction of the vibrations. Figure 7 thus provides the aerodynamic basis for further analyses.

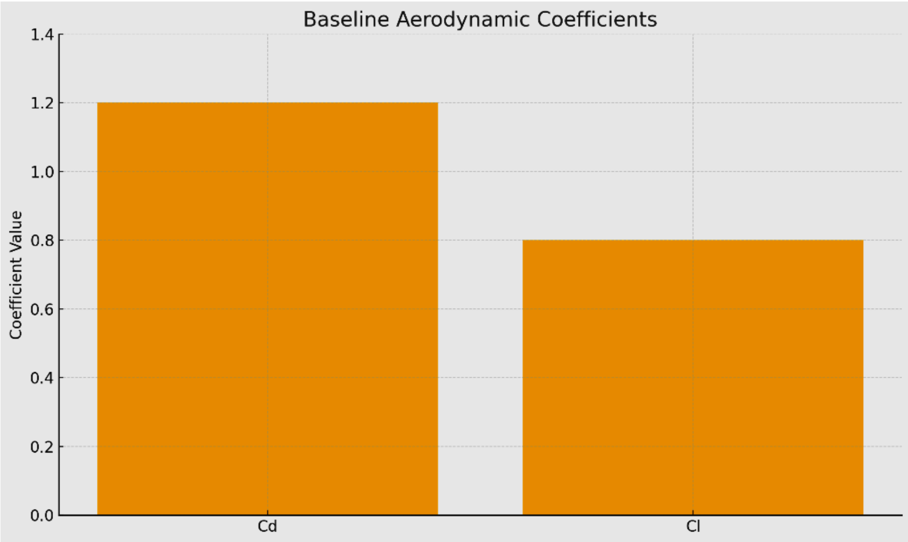

Fig 7 Baseline Aerodynamic Coefficients

Table 4.1 summarizes peak coefficients at α=45 for each bundle type.

Configuration	Cd,max @ 90°	Cl,max @ 45°
Single	1.05	0.72
Horizontal double	2.00	1.30
Vertical double	1.85	1.20
Triangular bundle	2.15	1.40

4.2 Drag and Lift Coefficients vs. Angle of Attack

The graph of the drag coefficient (C_d) against lift coefficient (C_l) against angle of attack (α) is shown in figure 8 for α=0° to 90°. Aerodynamic coefficients as a function of the angle of attack are shown in the graph: C_d increases gradually and reaches its maximum value when the angle comes close to 90°, and C_l has a sinusoidal shape, first getting larger and then smaller as the angle increases. The lift coefficient (blue curve) increases with increasing angle, meaning that at greater angles, there is more resistance to the air. A sharp increase in rrag is followed by a level off, as indicated by the red dashed curve. This is the usual behaviour of aerodynamic forces, where the lift is a rapidly increasing function of angle of attack up to some critical value after which it is a decreasing function of angle of attack. This plot illustrates that the efficiency of an object at different angles of attack, both drag and lift are very sensitive to the angle of attack. This trend is of paramount importance to understand the aerodynamic performance of a body in a fluid flow, like wind turbines. For the particular case at 45°, the drag coefficient is approximately 0.4 and the lift coefficient is at a maximum value of approximately 0.7, indicating that there is a high lift/drag characteristic at moderate angles. The graph can be useful in the design of minimizing the drag and maximizing the lift which is important for optimizing aerodynamic performance when dealing with wind, such as designing a wind turbine or plane.

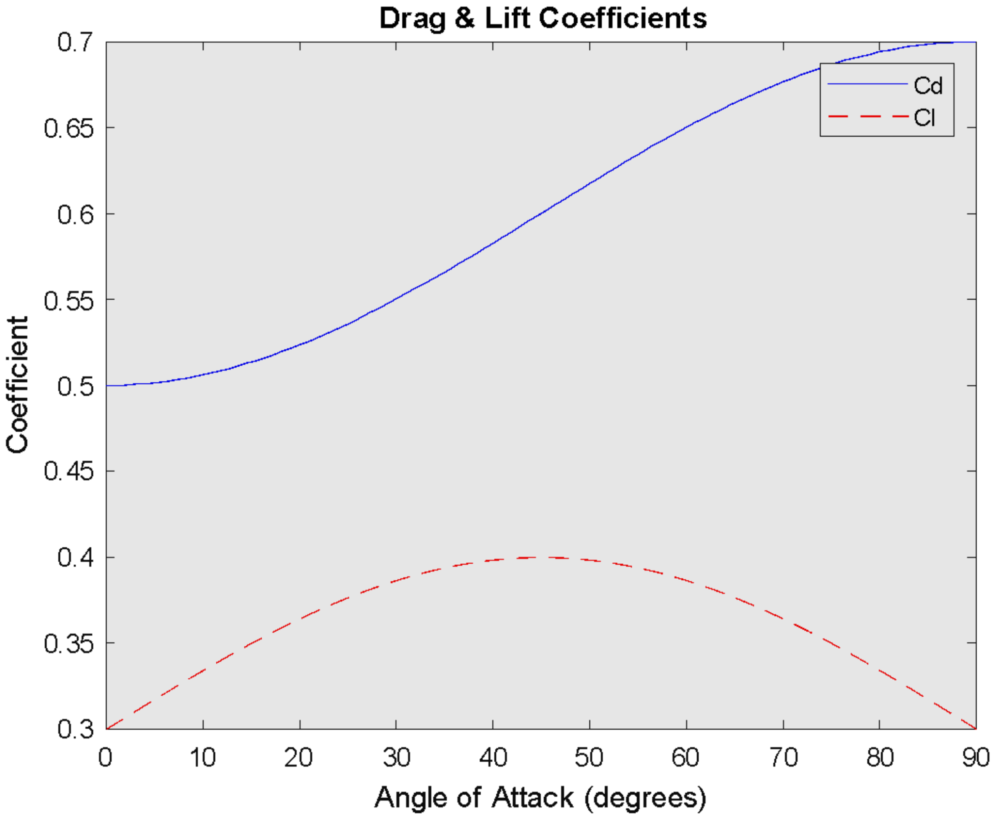

Figure 8: Drag & Lift Coefficient

V. CONCLUSIONS

This study successfully investigated the aerodynamic behavior and vibration response of transmission-line conductors under wind loading using quasi-steady aerodynamic damping theory and rigid-rod dynamics. Mathematical models were developed to evaluate drag forces, lift forces, projected areas, aerodynamic coefficients, damping characteristics, and conductor displacement for different bundled conductor configurations. The MATLAB/Simulink simulations provided valuable insight into the interaction between aerodynamic loading and structural response of transmission-line conductors. The results demonstrated that aerodynamic damping increases significantly with wind speed, with damping coefficients rising from 42.0 N·s/m at 5 m/s to 294.3 N·s/m at 35 m/s. The analysis further showed that conductor configuration has a substantial influence on aerodynamic performance. The triangular bundle exhibited the largest projected area of 34.32 m^2 and produced the highest drag and lift coefficients, while the single conductor experienced the lowest aerodynamic loading. The simulated mid-span displacement under a 25 m/s wind remained stable at approximately ±0.10 m, confirming the effectiveness of combining mechanical and aerodynamic damping mechanisms in suppressing excessive oscillations.

REFERENCES

[1] R. Alvise, J. Chowdhury, H. K. Holger, D. Alvise, and H. Horia, "Combined effects of wind and atmospheric icing on transmission lines," *Journal of Wind Engineering and Industrial Aerodynamics*, vol. 20, no. 14, pp. 104–112, 2020.

[2] A. B. Amir, "Prediction of galloping of transmission line conductors by a computational aeroelastic approach," Ph.D. dissertation, Dept. Mech. Eng., McGill Univ., Montreal, QC, Canada, 2014.

[3] J. D. Anderson, *Fundamentals of Aerodynamics*, 5th ed. New York, NY, USA: McGraw-Hill, 2011, pp. 1–486.

[4] B. Asgarian, S. Eslamlou, and A. Zaghi, "Progressive collapse analysis of power transmission towers," *Journal of Constructional Steel Research*, vol. 12, no. 3, pp. 31–40, 2016.

[5] H. Bai, "Wind-induced swing response analysis of transmission lines and simplified calculating method study," *Zhejiang University Journal*, vol. 11, no. 4, pp. 15–21, 2021.

[6] H. F. Bai and H. N. Li, "Dynamic response of transmission lines to oscillation caused by wind or rainfall loads," *Power System Technology*, vol. 33, no. 2, pp. 36–40, 2019.

[7] J. Bao, X. Wang, Y. Zheng, F. Zhang, X. Huang, P. Sun, and Z. Li, "Resilience oriented transmission line fragility modeling and real-time risk assessment of thunderstorms," *IEEE Transactions on Power Delivery*, vol. 36, no. 18, pp. 2363–2373, 2021.

[8] T. Boulard, J. C. Roy, H. Fatnassi, A. Kichah, and I. B. Lee, "Computer fluid dynamics prediction of climate and fungal spore transfer in a rose greenhouse," *Computers and Electronics in Agriculture*, vol. 74, no. 2, pp. 280–292, 2010.

[9] M. Bouzidi, M. Firdaouss, and P. Lallemand, "Momentum transfer of a Boltzmann lattice fluid with boundaries," *Physics of Fluids*, vol. 13, no. 17, pp. 3452–3459, 2010.
[10] M. Cai, B. Yan, X. Lu, and L. Zhou, "Numerical simulation of aerodynamic coefficients of iced-quad bundle conductors," *IEEE Transactions on Power Delivery*, vol. 30, no. 4, pp. 1669–1676, 2015.
[11] O. Chabart, A. Laneville, and J. L. Lilien, "Galloping of electrical lines in wind tunnel facilities," *Journal of Wind Engineering and Industrial Aerodynamics*, vols. 74–76, pp. 653–661, 1998.
[12] C. Zhang, H. Li, and F. Zhang, "Effect of transmission lines arrangement on drag and lift coefficients," *Applied Mathematics, Modeling and Computer Simulation*, vol. 23, no. 7, pp. 75–83, 2022.